Localization dynamics in multi-dimensional networks

Alexander Moroz

Wave-scattering.com

wavescattering@yahoo.com

(In collaboration with L. J. Maczewsky, K. Wang, A. A. Dovgiy, A. E. Miroshnichenko, M. Ehrhardt, M. Heinrich, D. N. Christodoulides, A. Szameit, and A. A. Sukhorukov)

(based on arXiv:1903.07883)

AAMP XVI, September 11, 2019

Overview

- Motivation: overcome the fundamental limit of the maximum of three spatial dimensions in experiments

Overview

- Motivation: overcome the fundamental limit of the maximum of three spatial dimensions in experiments
- Mapping from N to 1D preserving exact dynamics of a selected anchor site

Overview

- Motivation: overcome the fundamental limit of the maximum of three spatial dimensions in experiments
- Mapping from N to 1D preserving exact dynamics of a selected anchor site
- Dynamics associated with high dimensions

Overview

- Motivation: overcome the fundamental limit of the maximum of three spatial dimensions in experiments
- Mapping from N to 1D preserving exact dynamics of a selected anchor site
- Dynamics associated with high dimensions
- Bound states at the edge of the continuum (**BSEC**) - a fundamentally nontrivial addition the bound states in the continuum (**BIC**) - are shown to occurs exclusively in $D \geq 4$

Overview

- Motivation: overcome the fundamental limit of the maximum of three spatial dimensions in experiments
- Mapping from N to 1D preserving exact dynamics of a selected anchor site
- Dynamics associated with high dimensions
- Bound states at the edge of the continuum (**BSEC**) - a fundamentally nontrivial addition the bound states in the continuum (**BIC**) - are shown to occurs exclusively in $D \geq 4$
- Conclusions

Motivation - our limited goal

- General aim is to **achieve a perfect one-to-one reproduction of the entire multi-dimensional lattice in synthetic space**. However, this inevitably comes at the steep cost of exponentially increasing complexity when attempting to access higher dimensions.

Motivation - our limited goal

- General aim is to **achieve a perfect one-to-one reproduction of the entire multi-dimensional lattice in synthetic space**. However, this inevitably comes at the steep cost of exponentially increasing complexity when attempting to access higher dimensions.
- Our modest goal for a single anchor site: tailor the tridiagonalization by choosing a specific initial vector $\mathbf{v}_1 = |m_d\rangle$, where $|m_d\rangle$ represents the anchor site in the multi-dimensional lattice.

Motivation - our limited goal

- General aim is to **achieve a perfect one-to-one reproduction of the entire multi-dimensional lattice in synthetic space**. However, this inevitably comes at the steep cost of exponentially increasing complexity when attempting to access higher dimensions.
- Our modest goal for a single anchor site: tailor the tridiagonalization by choosing a specific initial vector $\mathbf{v}_1 = |m_d\rangle$, where $|m_d\rangle$ represents the anchor site in the multi-dimensional lattice.
- We show that arbitrary Hermitian multi-dimensional lattices with any local or non-local coupling distribution can be mapped to a 1D lattice with judiciously tailored nearest-neighbour couplings and detunings, such that **the dynamics at a chosen anchor site is faithfully reproduced** by the first site of the 1D lattice.

- A linear Hermitian Hamiltonian $\mathbf{H}$ and a local defect with a "detuning" ρ in the form of a *substitutional* impurity at site $m_{\rm d}$,

$$
{\rm i}\frac{{\rm d}\Psi_m}{{\rm d}t} = \sum_{m'} \mathbf{H}_{m,m'}\Psi_{m'} + \rho\delta_{m,m_{\rm d}}\Psi_m,
$$

t is the normalised time coordinate, m labels lattice sites, Ψ_m are complex wave function amplitudes, $\delta_{m,m_{\rm d}}$ is the Kronecker delta

- A linear Hermitian Hamiltonian $\mathbf{H}$ and a local defect with a "detuning" ρ in the form of a *substitutional* impurity at site m_d,

$$\mathrm{i}\frac{\mathrm{d}\Psi_m}{\mathrm{d}t} = \sum_{m'} \mathbf{H}_{m,m'}\Psi_{m'} + \rho\delta_{m,m_\mathrm{d}}\Psi_m,$$

  t is the normalised time coordinate, m labels lattice sites, Ψ_m are complex wave function amplitudes, δ_{m,m_d} is the Kronecker delta
- The Lanczos method determines a unitary transformation $\mathbf{V}$ relating $\mathbf{H}$ to a three-diagonal Hamiltonian $\mathbf{H}^{(3)} = \mathbf{V}^*\mathbf{H}\mathbf{V}$ corresponding to a 1D lattice with nearest-neighbour coupling by considering single-site excitations at the anchor defect site m_d as the initial step for a recursive Lanczos algorithm,

$$\mathrm{i}\frac{\mathrm{d}\Phi_m}{\mathrm{d}t} = \epsilon_m\Phi_m + C_{m-1}\Phi_{m-1} + C_m\Phi_{m+1} + \rho\delta_{m,1}\Phi_m = \sum_{m=1}^{N} \mathbf{H}^{(3)}_{nm}\Phi_m,$$

  where for $m \geq 1$, ϵ_m and C_m are the respective on- and off-diagonal elements of $\mathbf{H}^{(3)}$

3D to 1D example

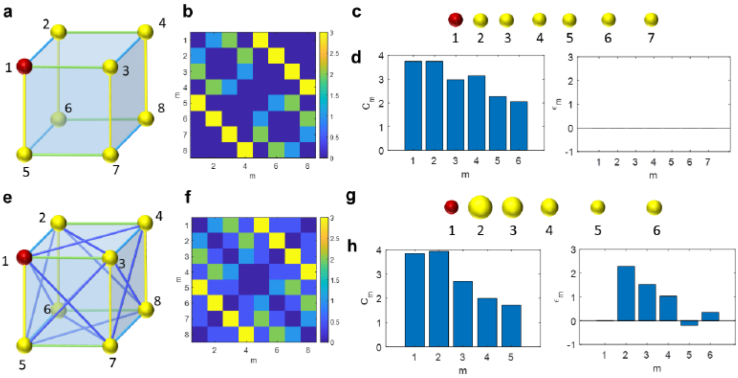

(a) Sketch of a 3D cubic structure with inhomogeneous nearest-neighbour-only couplings, with different coupling values denoted by lines with different colors. An anchor site (numbered 1) is marked red. (b) The Hamiltonian of the 3D structure in (a), where on-site detunings are all zero. (c) Sketch of the 1D equivalent lattice mapped from the 3D structure in (a). (d) The coupling constants C_m (left) and on-site detunings ϵ_m (right) of the 1D lattice in (c). (e) Sketch of the similar 3D structure as (a) with additional diagonal couplings. (f) Hamiltonian of the 3D structure in (e). (g) Sketch of the 1D lattice mapped from (e). (h) The coupling constants C_m (left) and on-site detunings ϵ_m (right) of the 1D lattice shown in (g).

Mapping peculiarities

- Generally, the number of sites in the 1D equivalent lattice is equal to the number of unique elements in the set of eigenvalues $\{\lambda_n\}$ of H, that have *non-zero* local density of states at the anchor site.

Mapping peculiarities

- Generally, the number of sites in the 1D equivalent lattice is equal to the number of unique elements in the set of eigenvalues $\{\lambda_n\}$ of H, that have *non-zero* local density of states at the anchor site.
- In the 1D equivalent lattice, there can be a *smaller* number of sites than in the multidimensional lattice that it is mapped from. There are two sources of site-number reduction:

Mapping peculiarities

- Generally, the number of sites in the 1D equivalent lattice is equal to the number of unique elements in the set of eigenvalues $\{\lambda_n\}$ of H, that have *non-zero* local density of states at the anchor site.
- In the 1D equivalent lattice, there can be a *smaller* number of sites than in the multidimensional lattice that it is mapped from. There are two sources of site-number reduction:
  - (i) the degeneracy of eigenvalues, since several degenerate modes will be mapped to one particular eigenfunction superposition that would be excited at the input, while the amplitudes and relative phases of such modes remain unchanged during propagation

Mapping peculiarities

- Generally, the number of sites in the 1D equivalent lattice is equal to the number of unique elements in the set of eigenvalues $\{\lambda_n\}$ of H, that have *non-zero* local density of states at the anchor site.
- In the 1D equivalent lattice, there can be a *smaller* number of sites than in the multidimensional lattice that it is mapped from. There are two sources of site-number reduction:
  - (i) the degeneracy of eigenvalues, since several degenerate modes will be mapped to one particular eigenfunction superposition that would be excited at the input, while the amplitudes and relative phases of such modes remain unchanged during propagation
  - (ii) the eigenmodes with vanishing local density of states at the anchor site, since such states would not be excited and are effectively removed from the mapping to 1D

4D to 1D example

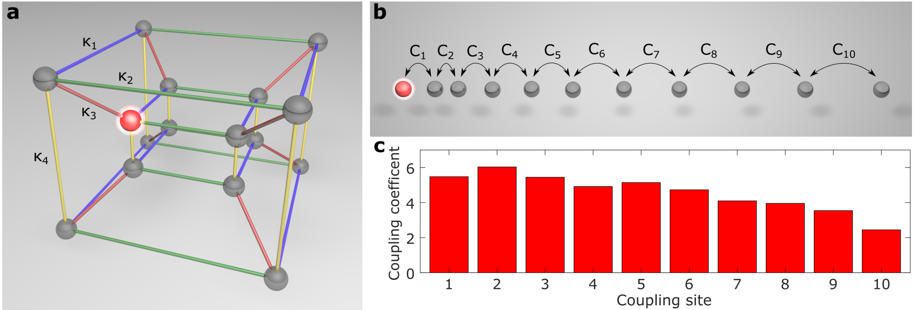

(a) Sketch of a four-dimensional tesseract (3D projection of the structure), where spheres mark the discrete sites and the connecting lines between them indicate the couplings $\kappa_1 = 1$, $\kappa_2 = 2$, $\kappa_3 = 3$, and $\kappa_4 = 4$. (b) The 1D mapping of this 4D object, where the excitation dynamics of first site is the same as for the corresponding red anchor site in (a). (c) The nearest-neighbour coupling coefficients C_m of the one-dimensional mapped lattice.

4D to 1D example

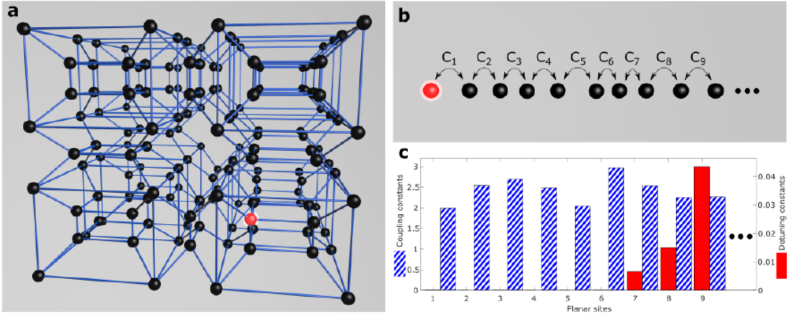

(a) Sketch of a multi-dimensional network of coupled four-dimensional hypercubes (tesseracts) shown in a 3D projection, where the black spheres mark the discrete sites and the connecting lines between them indicate the equal couplings. (b) The 1D mapping of this network, where the excitation dynamics of first site is the same as for the corresponding red anchor site in (a). (c) The nearest-neighbour coupling coefficients C_m (blue dashed) and the on-site detunings ϵ_m (red filled) of the 1D mapped lattice.

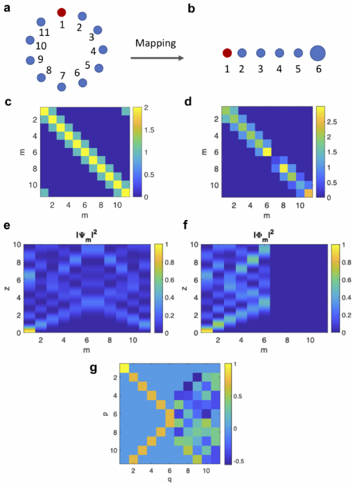

Example of mapping a two-dimensional ring lattice of 11 sites (a) to a one-dimensional lattice of 6 sites (b). The Hamiltonian of the original lattice H and the mapped lattice $H^{(3)}$ are plotted in (c) and (d), respectively. (e,f) The dynamics of all sites when the anchor (first) site is excited, in (e) the original lattice and (f) the mapped lattice. (g) Elements $V_{p,q}$ of the matrix V that describes the mapping, $H^{(3)} = V^{\dagger} H V$.

2D to 1D example - an experimental verification

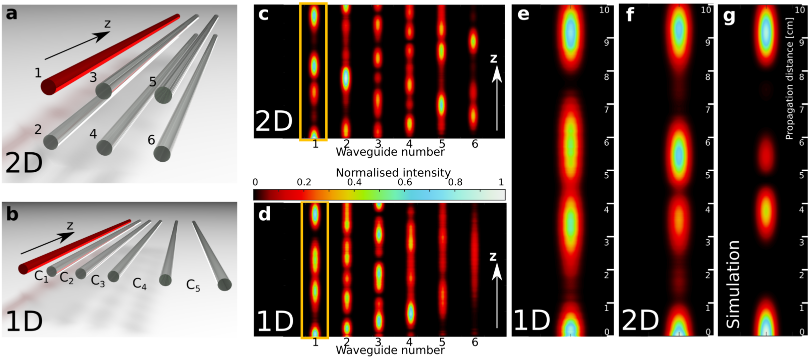

(a) Schematic of a 2D square lattice with equal horizontal and vertical couplings, and (b) the mapped 1D lattice with its non-uniform coupling distribution C_n implemented by different spacings. (c,d) Experimentally observed propagation dynamics in the experimentally realized 2D and 1D arrays. The arrows denote the propagation direction z along the waveguides. The 2D structure has been inscribed at a tilt angle of 20 to allow each lattice site to be viewed without obstruction or overlay. (e) Zoomed-in views of the anchor waveguide in the 2D lattice, (f) the first waveguide in the 1D equivalent lattice, and (g) tight-binding simulation. Note that the equivalent structure matches the anchor site dynamics remarkably well, such that the observed intensity distributions in them are more similar to one another than either of them is to the behaviour predicted by the tight-binding approximation.

Dynamics associated with N_d-dimensional hypercubes with a single defect

- Having verified mapping viability, investigate dynamics associated with high dimensions

Dynamics associated with N_d-dimensional hypercubes with a single defect

- Having verified mapping viability, investigate dynamics associated with high dimensions
- From now on, only periodic *hypercubic* lattices with a constant nearest-neighbour coupling $\widetilde{C}_{N_\mathrm{d}}$ factorised as $\widetilde{C}_{N_\mathrm{d}} = \widetilde{C}/N_\mathrm{d}$. This ensures that the respective systems exhibit photonic bands in the same interval $2\widetilde{C} < \beta < 2\widetilde{C}$ in order to allow for a direct comparison of effects associated with the multi-dimensional diffraction relation $\beta = 2\widetilde{C}\sum_{n=1}^{N_\mathrm{d}} \cos(k_n)$, where $\mathbf{k} = (k_1, k_2, \ldots, k_{N_\mathrm{d}})$ is the wave vector of the Bloch waves and β is the propagation constant.

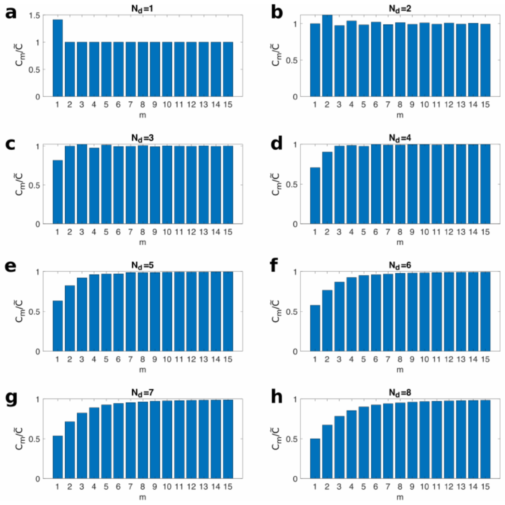

Normalized coupling coefficients ($C_m/\tilde{C}$) for the mapped 1D structure from N_d-dimensional lattices as indicated by labels, shown for the first 16 sites.

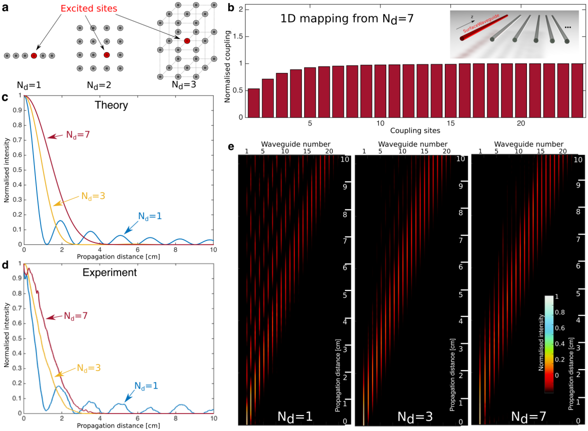

(a) Sketch of 1D, 2D and 3D lattices, each with an anchor site marked in red. (b) Calculated normalized coupling coefficients ($C_m/\widetilde{C}$) at the first 24 sites of a 1D structure mapped from an $N_{\rm d} = 7$ lattice. Inset: Schematic of the experimental realisation with appropriate inhomogeneous spacings between adjacent waveguides. (c,d) Dynamics of intensities at the excited sites for $N_{\rm d} = 1, 3, 7$: (c) theory and (d) experimental observations in the first waveguides of the mapped 1D lattices with $\widetilde{C} = 1\ {\rm cm}^{-1}$. (e) Fluorescence images of the propagation dynamics in the 1D mapped lattices corresponding to the dimensionalities $N_{\rm d} = 1, 3,$ and 7.

Dynamics

- The dynamics resulting from a single-site excitation in the *defect-free* case represents the (spatial) Green's function

$$G_{N_{\rm d}}(z) = \Phi_1(z)/\Phi_1(z=0) = [J_0(2\widetilde{C}_{N_{\rm d}} z)]^{N_d}$$

which effectively characterizes the response of the entire lattice

Dynamics

- The dynamics resulting from a single-site excitation in the *defect-free* case represents the (spatial) Green's function

$$G_{N_\mathrm{d}}(z) = \Phi_1(z)/\Phi_1(z=0) = [J_0(2\widetilde{C}_{N_\mathrm{d}} z)]^{N_d}$$

which effectively characterizes the response of the entire lattice
- The wavefunction at the anchor site is $\Phi_1(z) = G_{N_\mathrm{d}}(z)$ for a unit-amplitude excitation at the anchor site

Dynamics

- The dynamics resulting from a single-site excitation in the *defect-free* case represents the (spatial) Green's function

$$G_{N_{\rm d}}(z) = \Phi_1(z)/\Phi_1(z=0) = [J_0(2\widetilde{C}_{N_{\rm d}} z)]^{N_d}$$

  which effectively characterizes the response of the entire lattice
- The wavefunction at the anchor site is $\Phi_1(z) = G_{N_{\rm d}}(z)$ for a unit-amplitude excitation at the anchor site
- The frequency-domain (corresponding to wavenumber-space for waveguides lattices) Green's function is

$$\tilde{G}_{N_d}(\beta) = -\mathrm{i}\int_0^\infty e^{\mathrm{i}\beta z}[J_0(2\widetilde{C}_{N_{\rm d}} z)]^{N_d}\, dz = \int_0^\infty e^{-\beta z}[I_0(\widetilde{C}_{N_{\rm d}} z)]^{N_d}\, dz$$

- The dynamics resulting from a single-site excitation in the *defect-free* case represents the (spatial) Green's function

$$G_{N_\mathrm{d}}(z) = \Phi_1(z)/\Phi_1(z=0) = [J_0(2\widetilde{C}_{N_\mathrm{d}} z)]^{N_d}$$

which effectively characterizes the response of the entire lattice
- The wavefunction at the anchor site is $\Phi_1(z) = G_{N_\mathrm{d}}(z)$ for a unit-amplitude excitation at the anchor site
- The frequency-domain (corresponding to wavenumber-space for waveguides lattices) Green's function is

$$\tilde{G}_{N_d}(\beta) = -\mathrm{i}\int_0^\infty e^{\mathrm{i}\beta z}[J_0(2\widetilde{C}_{N_\mathrm{d}} z)]^{N_d}\, dz = \int_0^\infty e^{-\beta z}[I_0(\widetilde{C}_{N_\mathrm{d}} z)]^{N_d}\, dz$$

- The presence of a defect ρ at the anchor site acts as an effective distributed source along the waveguide,

$$\Phi_1(z) = G_{N_\mathrm{d}}(z) + i\rho\int_0^z G_{N_\mathrm{d}}(z-z')\,\Phi_1(z')\, dz'$$

Localized defect modes

- Knowledge of the Green's function in a defect-free lattice allows us to predict the localisation behaviour upon introduction of a defect (substitutional impurity) as

$$\rho = 1/\widetilde{G}_{N_{\mathrm{d}}}(\beta_{\mathrm{d}})$$

where β_{d} is the propagation constant of a localised defect mode.

Localized defect modes

- Knowledge of the Green's function in a defect-free lattice allows us to predict the localisation behaviour upon introduction of a defect (substitutional impurity) as

$$\rho = 1/\widetilde{G}_{N_{\mathrm{d}}}(\beta_{\mathrm{d}})$$

  where β_{d} is the propagation constant of a localised defect mode.
- Real-valued detunings ρ can support localization in the photonic band-gap, where $\mathrm{Im}\,\widetilde{G}_{N_{\mathrm{d}}}(\beta) = 0 \Longrightarrow \mathrm{Im}\,\widetilde{G}_{N_{\mathrm{d}}}(\beta)$ reflects this tendency of light to remain localised in the excited anchor site.

Localized defect modes

- Knowledge of the Green's function in a defect-free lattice allows us to predict the localisation behaviour upon introduction of a defect (substitutional impurity) as

$$\rho = 1/\widetilde{G}_{N_{\rm d}}(\beta_{\rm d})$$

where $\beta_{\rm d}$ is the propagation constant of a localised defect mode.

- Real-valued detunings ρ can support localization in the photonic band-gap, where $\mathrm{Im}\,\widetilde{G}_{N_{\rm d}}(\beta) = 0 \Longrightarrow \mathrm{Im}\,\widetilde{G}_{N_{\rm d}}(\beta)$ reflects this tendency of light to remain localised in the excited anchor site.
- The *excitation efficiency* for the localised defect mode = the fraction of power remaining at the input site after a sufficiently long evolution. In the theoretical limit of $z \to +\infty$, it is expressed as:

$$\eta = \left(\frac{\partial \rho}{\partial \beta_{\rm d}}\right)^{-2}$$

From localised defect modes to BSEC

- The localized modes appear at the photonic band-edge in lattices of any dimensionality

From localised defect modes to BSEC

- The localized modes appear at the photonic band-edge in lattices of any dimensionality
- For conventional dimensions $N_d \leq 3$, the band-edge modes extend throughout the lattice and accordingly $\eta = 0$

From localised defect modes to BSEC

- The localized modes appear at the photonic band-edge in lattices of any dimensionality
- For conventional dimensions $N_d \leq 3$, the band-edge modes extend throughout the lattice and accordingly $\eta = 0$
- For $N_d \geq 4$, the excitation efficiency instantly attains a finite non-zero value at the critical defect strength $===>$ Bound states at the edge of the continuum (**BSEC**) - a fundamentally nontrivial addition the bound states in the continuum (**BIC**)

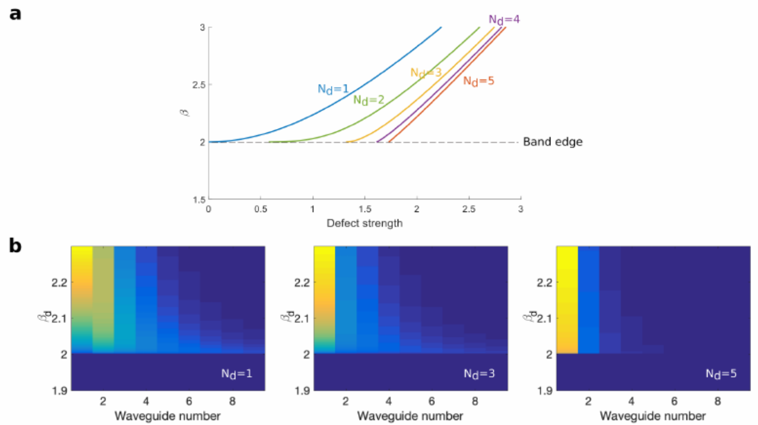

(a) Theoretical plot of the defect state propagation constant β_d versus the defect strength ρ. (b) Color plot illustrating the dependence of the population in the first nine waveguides (horizontal axis) of the mapped structure on the propagation constant β_d (vertical axis) of the defect state for $N_d = 1, 3$ and 5.

BSEC analysis

- The band-edge corresponds to the branch point at $\beta = N_d$ of the LT integral, $\tilde{G}_{N_d}(\beta) = \int_0^\infty e^{-\beta z}[I_0(\widetilde{C}_{N_\mathrm{d}} z)]^{N_d}\, dz$, and we are interested only in the band-gap region

- The band-edge corresponds to the branch point at $\beta = N_d$ of the LT integral, $\tilde{G}_{N_d}(\beta) = \int_0^\infty e^{-\beta z} [I_0(\widetilde{C}_{N_\mathrm{d}} z)]^{N_d}\, dz$, and we are interested only in the band-gap region
- Given

$$I_\nu(z) \sim \frac{e^z}{\sqrt{2\pi z}}, \qquad |\arg z| \leq \pi/2 - \delta$$

investigate the qualitative behaviour of $\tilde{G}_{N_d}(\beta)$ in N_d dimensions where Re $\beta \geq N_d$ approaches a band-edge

BSEC analysis

- The band-edge corresponds to the branch point at $\beta = N_d$ of the LT integral, $\tilde{G}_{N_d}(\beta) = \int_0^\infty e^{-\beta z}[I_0(\widetilde{C}_{N_\mathrm{d}} z)]^{N_d}\, dz$, and we are interested only in the band-gap region
- Given
$$I_\nu(z) \sim \frac{e^z}{\sqrt{2\pi z}}, \qquad |\arg z| \le \pi/2 - \delta$$
investigate the qualitative behaviour of $\tilde{G}_{N_d}(\beta)$ in N_d dimensions where Re $\beta \ge N_d$ approaches a band-edge
- At the same time, $I_\nu(z)$ ($\nu \ge 0$) is positive and monotonically increasing (from $I_0(0) = 1$ for $\nu = 0$) to infinity

BSEC analysis - II

- With $\Delta = \beta - N_d \geq 0$ being the distance of β to the branch point at N_d, one has in virtue of the positivity, monotonicity, and the leading asymptotic of $I_0(z)$ for $z \to \infty$ for sufficiently large a (up to a proportionality constant)

$$\tilde{G}_{N_d}(\beta) \sim \int_a^\infty e^{-\Delta z} z^{-N_d/2}\, dz$$

BSEC analysis - II

- With $\Delta = \beta - N_d \geq 0$ being the distance of β to the branch point at N_d, one has in virtue of the positivity, monotonicity, and the leading asymptotic of $I_0(z)$ for $z \to \infty$ for sufficiently large a (up to a proportionality constant)

$$\tilde{G}_{N_d}(\beta) \sim \int_a^\infty e^{-\Delta z} z^{-N_d/2}\, dz$$

- Because $\int_0^a e^{-\beta z}[I_0(z)]^{N_d}\, dz$ is a finite number, one sees immediately that at the band edge $\tilde{G}_{N_d}(N_d)$ in 1D and 2D diverges and is finite for $N_d = 3$

BSEC analysis - II

- With $\Delta = \beta - N_d \geq 0$ being the distance of β to the branch point at N_d, one has in virtue of the positivity, monotonicity, and the leading asymptotic of $I_0(z)$ for $z \to \infty$ for sufficiently large a (up to a proportionality constant)

$$\tilde{G}_{N_d}(\beta) \sim \int_a^\infty e^{-\Delta z} z^{-N_d/2} \, dz$$

- Because $\int_0^a e^{-\beta z} [I_0(z)]^{N_d} \, dz$ is a finite number, one sees immediately that at the band edge $\tilde{G}_{N_d}(N_d)$ in 1D and 2D diverges and is finite for $N_d = 3$
- $\Longrightarrow$ localized modes appear in 1D and 2D for any defect strength, whereas for $N_d \geq 3$ a critical defect magnitude, $\rho \geq \rho_{cr}$, is required.

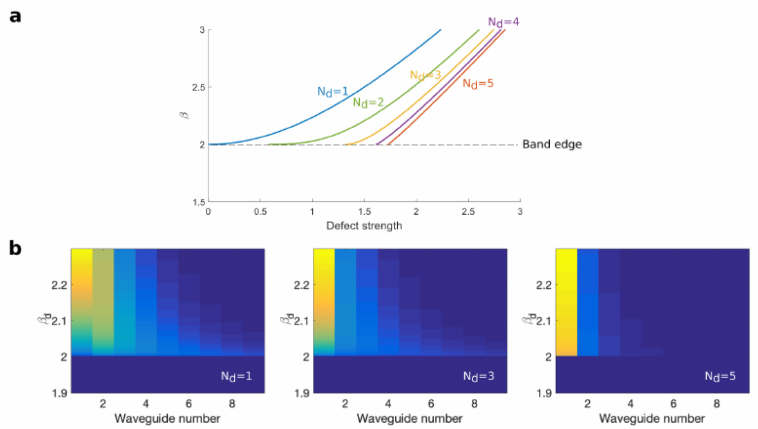

(a) Theoretical plot of the defect state propagation constant β_d versus the defect strength ρ. (b) Color plot illustrating the dependence of the population in the first nine waveguides (horizontal axis) of the mapped structure on the propagation constant β_d (vertical axis) of the defect state for $N_d = 1, 3$ and 5.

BSEC argument

One can easily argue that $N_d = 4$ is the first dimension for which the excitation efficiency $\eta = \partial_\beta \tilde{G}_{N_d}(\beta)/[\tilde{G}_{N_d}(\beta)]^2$ at the band edge will be *finite*.

By performing the derivative in the LT integral one finds that the derivative tail for sufficiently large a is

$$\int_a^\infty e^{-\Delta z} z^{1-N_d/2}\, dz. \tag{1}$$

But this coincides with the tail of $\tilde{G}_{N_d}$ in the dimension $N_d - 1$. Knowing that (the tail of) $\tilde{G}_{N_d}(N_d)$ diverges for $N_d = 0, 1, 2$ and is finite for $N_d = 3$, the derivative of $\tilde{G}_{N_d}(N_d)$ diverges for $N_d = 1, 2, 3$ and is finite for $N_d \geq 4$. Hence the excitation efficiency η at the band edge is zero for $N_d = 1, 2, 3$ and becomes finite beginning with $N_d = 4$.

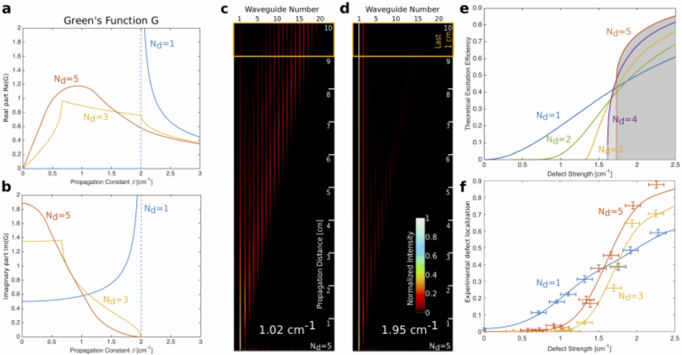

(c),(d) Fluorescence images of the mapped $N_\mathrm{d} = 5$ lattices with a defect: (c) below the localisation threshold, for a detuning of $1.02\,\mathrm{cm}^{-1}$, light is able to escape; (d) above the localisation threshold, for a detuning $1.95\,\mathrm{cm}^{-1}$, the initial excitation remains largely localized. (f) Experimentally observed localisation at the defect (symbols) compared with the theoretical predictions (lines) in the planar lattices with different mapped dimensionality $N_\mathrm{d} = 1, 3, 5$, defined as the average relative intensity in the last $1\,\mathrm{cm}$ of the first waveguide. To indicate the influence of random fabrication imperfections, the error bars are numerically derived from an ensemble of 300 realizations with Gaussian-distributed lattice parameters centered around the design values with their typical standard deviation of 10 %.

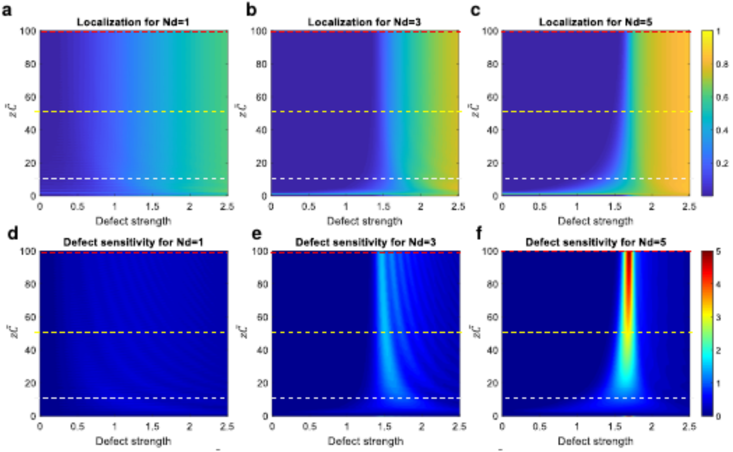

Theoretical analysis of the influence of finite propagation length onto multidimensional defect localization. (a–f) Color density plot of the (a–c) defect localization, $|\Phi_1(z)|^2$, and (d–f) defect sensitivity, defined as $\mathrm{d}|\Phi_1(z)|^2/\mathrm{d}\rho$, versus the defect strength (horizontal axis) and normalized propagation length $z\tilde{C}$ (vertical axis) for $N_d = 1, 3$ and 5, as indicated by labels.

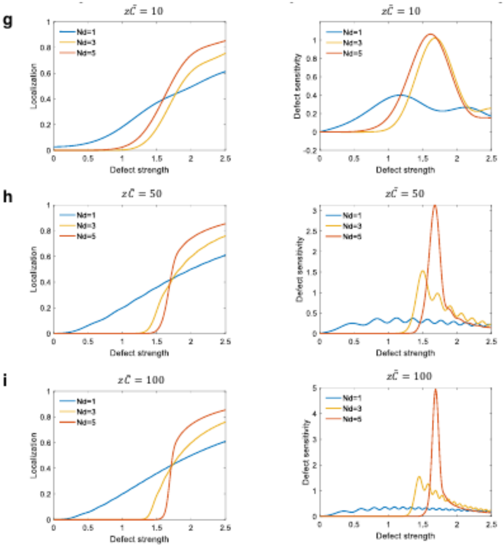

(g–i) Plots of the defect localization (left) and defect sensitivity (right) versus defect strength for the propagation lengths $z\tilde{C} = 10, 50$ and 100, respectively.

Conclusions

- Bound states at the edge of the continuum (**BSEC**) - a fundamentally nontrivial addition the bound states in the continuum (**BIC**) - are shown to occurs exclusively in $D \geq 4$

Conclusions

- Bound states at the edge of the continuum (**BSEC**) - a fundamentally nontrivial addition the bound states in the continuum (**BIC**) - are shown to occurs exclusively in $D \geq 4$
- BSEC giving rise to a sharp localization transition and an extreme increase of sensitivity with respect to the detuning of the respective anchor site

Conclusions

- Bound states at the edge of the continuum (**BSEC**) - a fundamentally nontrivial addition the bound states in the continuum (**BIC**) - are shown to occurs exclusively in $D \geq 4$
- BSEC giving rise to a sharp localization transition and an extreme increase of sensitivity with respect to the detuning of the respective anchor site
- Series of experimental verifications of the mapped equivalent lattices of up to 7D systems were implemented and corresponding dynamics was observed

Conclusions

- Bound states at the edge of the continuum (**BSEC**) - a fundamentally nontrivial addition the bound states in the continuum (**BIC**) - are shown to occurs exclusively in $D \geq 4$
- BSEC giving rise to a sharp localization transition and an extreme increase of sensitivity with respect to the detuning of the respective anchor site
- Series of experimental verifications of the mapped equivalent lattices of up to 7D systems were implemented and corresponding dynamics was observed
- Other tridiagonalization algorithms (e.g. the Householder transformation previously applied for isospectral mapping) do not allow for such an explicit choice

Conclusions

- Bound states at the edge of the continuum (**BSEC**) - a fundamentally nontrivial addition the bound states in the continuum (**BIC**) - are shown to occurs exclusively in $D \geq 4$
- BSEC giving rise to a sharp localization transition and an extreme increase of sensitivity with respect to the detuning of the respective anchor site
- Series of experimental verifications of the mapped equivalent lattices of up to 7D systems were implemented and corresponding dynamics was observed
- Other tridiagonalization algorithms (e.g. the Householder transformation previously applied for isospectral mapping) do not allow for such an explicit choice
- The concept of synthetic dimensions effectively extends the scope of experimental observations beyond the (3+1)-dimensional space-time and thereby opens up new opportunities in various physical contexts, from innovative light control to quantum information processing

- *High-dimensional synthetic lattice with enhanced defect sensitivity in planar photonic structures*, in Advanced Photonics 2018 (BGPP, IPR, NP, NOMA, Sensors, Networks, SPPCom, SOF), OSA Technical Digest, paper NpTh3I.3
- *Experimental realization of high dimensional synthetic lattices in planar photonic structures*, in 2018 Conference Conference on Lasers and Electro-Optics, OSA Technical Digest, paper JTh5B.7
- *Experimental Realization of Exact Mapping from Multi-Dimensional to Planar Micro-Photonic Lattices*, in 2017 European Conference on Lasers and Electro-Optics and European Quantum Electronics Conference, OSA Technical Digest, paper CK_13_1
- *Optical Simulation of Nonlinear Twisted-Ring Defect States with Planar Waveguide Arrays*, in Frontiers in Optics 2016, OSA Technical Digest, paper JTh2A.141
- *Optical simulation of multi-dimensional nonlinear defect states with planar waveguide arrays*, in Photonics and Fiber Technology 2016 (ACOFT, BGPP, NP), OSA Technical Digest, paper NTh1A.4

Thank you for your attention!